01 Oct 2023

Modulation Of Electrocatalytic Activity By Tuning Anion Electronegativity: Case Study With Copper Chalcogenides

Harish Singh

David Prendergast

Manashi Nath
Missouri University of Science and Technology, nathm@mst.edu

Recommended Citation

H. Singh et al., "Modulation Of Electrocatalytic Activity By Tuning Anion Electronegativity: Case Study With Copper Chalcogenides," *JPhys Energy*, vol. 5, no. 4, article no. 045016, IOP Publishing, Oct 2023.
The definitive version is available at https://doi.org/10.1088/2515-7655/ad040f

JPhys Energy

Modulation of electrocatalytic activity by tuning anion electronegativity: case study with copper chalcogenides

IOP Publishing J. Phys. Energy 5 (2023) 045016 https://doi.org/10.1088/2515-7655/ad040f

Journal of Physics: Energy

OPEN ACCESS

RECEIVED
29 March 2023

REVISED
21 September 2023

ACCEPTED FOR PUBLICATION
17 October 2023

PUBLISHED
30 October 2023

PAPER

Modulation of electrocatalytic activity by tuning anion electronegativity: case study with copper chalcogenides

Harish Singh[1], **David Prendergast**[2] **and Manashi Nath**[1,*]

[1] Department of Chemistry, Missouri University of Science and Technology, Rolla, MO 65409, United States of America
[2] Joint Centre for Energy Storage Research, The Molecular Foundry, Lawrence Berkeley National Laboratory, Berkeley, CA 94720, United States of America
* Author to whom any correspondence should be addressed.

E-mail: nathm@mst.edu

Keywords: transition metal chalcogenides, oxygen evolution reaction (OER), electrocatalysis

Supplementary material for this article is available online

Abstract

Anion-tuning in metallic chalcogenides has been shown to have a significant impact on their electrocatalytic ability for overall water splitting. In this article, copper-based chalcogenides (Cu_2X, X = O, S, Se, and Te) have been systematically studied to examine the effect of decreasing anion electronegativity and increasing covalency on the electrocatalytic performance. Among the copper chalcogenides, Cu_2Te has the highest oxygen evolution reaction (OER) activity and can sustain high current density of 10 and 50 mA cm^{-2} for 12 h. The difference in intrinsic catalytic activity of these chalcogenide surfaces have been also probed through density functional theory calculations, which was used to estimate energy of the catalyst activation step. It was observed that the hydroxyl adsorption on the surface catalytic site is critically important for the onset and progress of OER activity. Consequently, it was also observed that the –OH adsorption energy can be used as a simple but accurate descriptor to explain the catalytic efficiency through volcano-like correlation plot. Such observation will have a significant impact on developing design principle for optimal catalytic surface exhibiting high performance as well as prolonged stability.

Transition metal chalcogenides have become increasingly important in the field of electrocatalysis for their unprecedented high efficiency in oxygen evolution reaction (OER) [1–6]. This reaction comprises a critical step for several electrochemical energy conversion processes including water splitting, fuel cells, and clean hydrogen generation [7]. Transition metal chalcogenides have been found to be particularly effective in promoting electrochemical energy conversion due to their unique electronic structure that facilitates interfacial charge transfer through modulation of electron density around the catalytically active site [8]. Transition metal chalcogenides typically containing one or more transition elements such as iron, cobalt, or nickel, combined with a chalcogen atom such as sulfur, selenium, or tellurium, frequently form layered structure [9]. Such layered morphology are expected to exhibit improved electrocatalytic efficiency owing to better accessibility to active sites, and facile intermediate adsorption on the surface. Such properties also lead to improved OER activity. Moreover, the electronic structure of metal chalcogenides is highly tunable through anion modulation, which leads to further tuning of their electrocatalytic properties [3, 10, 11]. This is especially useful for optimizing the OER, as the reaction is highly sensitive to the presence of certain metals and chalcogen atoms. Over the past several years, intense research has led to the identification of several transition metal chalcogenides which shows highly efficient OER activity [12–15]. Several transition metal chalcogenides comprising, Ni, Co, and Fe have also been identified from our previous research [8, 16–19]. During the course of these studies, it was further revealed that the anion electronegativity had a critical role to play in the observed OER electrocatalytic efficiency. Specifically, the electronegativity of the coordinated anion affects the ionicity or covalent strength of the *M-X* bond (*M-X*, where *M* refers to transition metal and X = S, Se, Te), respectively. The electrochemical redox of the transition metal site is more impacted by the covalent character of the *M-X* bonding, which ameliorates with bond strength [20]. Because the degree of

covalency in transition metal tellurides is higher than that of the corresponding selenides, most transition metal tellurides have the intrinsic property of enhanced metallicity, which can lead to better conductivity and charge transfer rate of the transition metal tellurides [21]. Additionally, transition metal chalcogenides are relatively inexpensive compared to precious metal based OER catalysts, which makes them attractive for large-scale applications. Moreover, metal chalcogenides exhibit excellent chemical stability, which is important for maintaining the activity of the electrode over time [16]. The chalcogens in the compounds form strong covalent bonds with the metal atoms, which renders the compounds resistant to corrosion or degradation. Improvements in electrocatalyst performance have been proposed through the use of a wide range of control mechanisms, including the development of hierarchical structures, the doping of heteroatoms and the processing of alloys [17, 22–25]. Few studies have also investigated the effect of anion species on the performance of water splitting electrocatalysts [16, 18, 26–28].

In our previous study, we have reported the effect of varying anion covalency in Ni-based chalcogenide [18]. Specifically, it was observed that electrocatalyst efficiency increased significantly down the chalcogen series resulting in telluride showing the highest OER efficiency. The electrocatalytic activity trend in these chalcogenides could be also comprehended in a manner akin to the Sabatier principle [29] by following the hydroxyl (–OH) adsorption energy on the catalyst surface. The initial –OH adsorption on the surface preceded by local oxidation of the active site comprises the activation step and in our previous studies we have proposed that this –OH adsorption energy can be used as a descriptor and correlated with the observed OER catalytic activity. Nevertheless, a systematic study of the variation of OER catalytic activity solely as a function of anion electronegativity and its correlation with changes in –OH adsorption energy is still missing. However, such insight is critically needed for developing effective catalyst design principles by elucidating how surface anion coordination alters catalyst activation and further charge transfer across the interface. By exploring the direct correlation between anion electronegativity and –OH adsorption energy in various catalytic systems, we can gain deeper insights into the reaction mechanisms, surface intermediates, and reaction kinetics involved in the OER.

In this article, we have investigated the variation of inherent electrocatalytic activity for a series of copper chalcogenides with generic formula, Cu_2X (X = O, S, Se, and Te). These copper chalcogenides show similar crystal structure. However, the OER catalytic activity shows a significant enhancement with decreasing anion electronegativity with Cu_2Te showing the best activity. Estimation of the –OH adsorption energy through density functional theory (DFT) calculations revealed its clear correlation with OER activity further confirming the appropriateness of using –OH adsorption energy as a descriptor for the OER efficiency. Furthermore, these copper chalcogenides can be optimized to provide both high catalytic activity and stability. The novelty of our research lies in the systematic study of the variation of OER catalytic activity based solely on the anion electronegativity. To the best of our knowledge, such a comprehensive analysis had been missing from the existing literature, and our work fills this critical gap. By understanding the impact of anion electronegativity on catalytic performance, we aim to unravel the underlying principles governing OER and contribute to the rational design of highly efficient catalyst surfaces.

1. Materials and method

The reagents were analytical grade and used as received. Copper (II) chloride dihydrate ($CuCl_2{\cdot}2H_2O$), copper sulphate ($CuSO_4.5H_2O$), copper (II) acetate $Cu(CH_3COO)_2$, tellurium (Te) powder, selenium (Se), and hydrazine hydrate ($N_2H_4{\cdot}H_2O$) were purchased from Acros Organics. Potassium hydroxide (KOH), potassium chloride (KCl), hydrochloric acid (HCl) and $RuCl_3$ were purchased from Fisher Scientific. Nafion was purchased from Ion Power, while carbon cloth (CC) substrate was purchased from Fuel Cells Etc. Corporation in College Station, Texas.

Synthesis of Cu_2Se: On the basis of the synthesis approach described in our earlier paper [10], copper selenide was synthesized by an enhanced hydrothermal process. In a typical synthesis procedure, powdered copper oxide (Cu_2O) and selenium (Se) were mixed in an equimolar ratio. The original molar ratio of Cu_2O to Se was chosen to be 1:1. First, 8 ml of deionized water was used to dissolve Cu_2O (0.001 M) in a Teflon-lined 23 ml acid digestion bomb. Se (0.001 M) was added to the mixture after mixing vigorously for 20 min. Finally, 3 ml of $N_2H_4.H_2O$ were added to the mixture, followed by 20 min of continuous stirring. The resulting solution was sealed in a stainless-steel autoclave lined with Teflon and heated at 185 °C for 24 h. After that, the autoclave was allowed to cool to room temperature naturally. The final product was then centrifuged and repeatedly washed with an ethanol and deionized water solution. Finally, a vacuum oven at 60 °C was used to dry the final product.

Synthesis of Cu_2Te: Cu_2Te were also synthesized following a similar protocol as above. In a typical synthesis procedure, powdered copper chloride ($CuCl_2.6H_2O$) and tellurium (Te) were mixed in a molar ratio of 2:1. Both Cu and Te precursors were added in 6 M KOH solution. Finally, 3 ml of $N_2H_4.H_2O$ were added to the mixture, followed by 20 min of continuous stirring. The final mixture was sealed and heated at 175 °C for 24 h in a Teflon-lined stainless-steel autoclave. The resultant products were recovered using centrifugation, and the final product was dried by heating at 60 °C .

Synthesis of Cu_2S: In a typical synthesis procedure, $CuSO_4.5H_2O$ (0.02 mol) was added to 8 ml of DMSO while the mixture was continuously stirred for 20 min to result in a clear, green solution. This mixture was poured in a Teflon-sealed autoclave and kept at 175 °C for 6 h. The resultant products were recovered using centrifugation, cleaned with ethanol and finally a vacuum oven at 60 °C was used to dry the final product.

Synthesis of Cu_2O: Typically, 1 mmol $Cu(CH_3COO)_2$ and 0.5 mmol glucose are dissolved in 8 ml of distilled water and stirred vigorously to form a blue dispersion. The resultant liquid was placed to a Teflon-lined stainless steel autoclave (23 ml). The autoclave was sealed and placed to 100 °C oven for 12 h before naturally cooling to ambient temperature. The resultant red solid products were recovered using centrifugation, cleaned with ethanol and finally a vacuum oven at 60 °C was used to dry the final product.

Electrode preparation: A homogenous catalyst ink was made by mixing 300 μl of ethanol with 0.8 ml of Nafion (5% by weight) and 2 mg of catalyst powder in order to study the OER activity of the hydrothermally synthesized catalyst. This mixture was homogenized into an ink using an ultrasonicator for about an hour. 100 μl of the ink was drop cast onto CC (geometric area of 0.283 cm^{-2}).

2. Characterization technique

The product was analyzed using powder x-ray diffraction (PXRD) with a Philips X-Pert and CuKα (1.5418 Å) radiation without any further purification. By employing a scanning electron microscope (SEM, Helios Hydra) with an acceleration voltage of 15 kV and a working distance of 10 mm, the morphology of the samples was examined. X-ray photoelectron spectroscopy (XPS) was used to determine the valence states of the elements and the chemical composition of the catalystsboth before and after the OER stability studies. X-ray photoelectron spectroscopy (XPS) analyses were conducted with a KRATOS AXIS 165 instrument, utilizing a monochromatic Al X-ray source. All XPS investigations were performed on the pristine catalyst surface without sputtering. An IviumStat potentiostat was used for all electrochemical studies. A graphite rod functioned as the counter electrode, saturated calomel electrode (SCE) as the reference electrode, and the copper-based chalcogenides loaded on CC substrate functioned as the working electrode during the electrochemical studies. Linear sweep voltammetry (LSV) curves were acquired at a scan rate of 5 mV s^{-1} and the electrochemical workstation automatically corrected the LSV via iR compensation. Electrochemical impedance spectroscopy (EIS) was used to examine the charge transfer resistance from 0.01 Hz to 100 kHz.

2.1. Tafel slope

The Tafel slope, which is determined by fitting polarization data to the Tafel equation, is a crucial measure for evaluating OER activity. The dependence of the overpotential on the current density j is represented by the Tafel equation, as shown in equation (1):

$$\eta = \mathrm{a} + \left(\frac{2.3\mathrm{RT}}{\alpha n F}\right) \log\ (\mathrm{j}) \tag{1}$$

where n is the number of electrons involved in the reaction, α is the transfer coefficient, and F is the Faraday constant. The Tafel slope is given by $2.3RT/\alpha nF$.

The formula for converting potentials measured with a SCE to reversible hydrogen electrode (RHE) potentials is:

$$\mathrm{E\,(RHE)} = \mathrm{E\,(SCE)} + \mathrm{E^{\circ}\,(SCE)} + 0.059\ \mathrm{pH} \tag{2}$$

where, E(RHE) is the potential in RHE scale. E(SCE) is the potential measured with the SCE. E°(SCE) is the standard potential of the SCE, which is typically considered to be 0.241 V at 25 °C. 0.059 is the conversion factor representing the Faraday constant (F) divided by 1000 (F/1000) to convert from volts to millivolts. Here, pH represents the pH value of the solution under consideration.

3. Computational details

The first-principles computations were carried out using the DFT as implemented in the Vienna ab initio simulation package [30]. The generalized gradient approximation using the Perdew–Burke–Ernzerhof function ((PAW)) was used to define the exchange correlation approximation [31, 32]. For the anticipated augmented wave approach, the plane-wave cut-off energy was 520 eV. To prevent erroneous interactions between periodic images, a supercell of $3 \times 3 \times 3$ matrix was built with the vacuum layer of 10 Å. The Brillouin zone integrations were performed using a $3 \times 3 \times 1$ Monkhorst–Pack grid for (001) surfaces. A conjugate gradient algorithm was used to iteratively relax all the ions, and the atomic forces of all systems were reduced to less than 0.01 eV. During the structure relaxation process, a Methfessel–Paxton smearing with a value of $\sigma = 0.05$ eV is applied to the orbital occupation. On the other hand, an accurate computation of the electronic structure was performed using a tetrahedron approach with Blöch corrections.

4. Results and discussion

The series of copper chalcogenides of generic formula, Cu_2X (X = S, Se, Te) along with Cu_2O were synthesized through one-pot solvothermal technique at temperatures between 175° and 185°. The series of copper chalcogenides, Cu_2Te, Cu_2Se, Cu_2S and Cu_2O were characterized through various structural, microscopy, and surface analysis techniques. Figures 1(a)–(d) shows the crystalline PXRD patterns of the hydrothermally synthesized series of copper-based chalcogenides. Each of these phases matched well with their corresponding standard diffraction patterns as shown in the corresponding PXRD plots, which also illustrates phase purity of these samples. The sharp diffraction peaks indicate high degree of crystallinity. Scanning electron microscopy (SEM) was used to study the morphological characteristics of Cu based metal chalcogenides. The SEM images of all four samples, as shown in inset of figures 2(a)–(d) and S1, showed globular-like nanoparticles with particle sizes ranging from 30 to 120 nm. XPS was used to analyze oxidation state of the elements and phase composition for these chalcogenides. In order to investigate the XPS survey spectrum for the Cu_2X sample, C1s peak (284.6 eV) was used as a reference. The high resolution XPS spectra of Cu in figures 2(a)–(d) shows that there is a spin-orbit splitting of 19.7 eV between the two peaks centered at 933.5 eV and 953.2 eV for all four copper based chalcogenides (Cu_2Te, Cu_2Se, Cu_2S, Cu_2O, respectively), which are identified as Cu 2p3/2 and Cu 2p1/2, respectively [33]. Compositions containing Cu in 2+ oxidation state with a d^9 ground state configuration are distinguished by Cu satellite peaks at 941.5 and 962.3 eV. It has been determined that the peaks at 576.6 eV and 586.8 eV in high resolution spectra of Te 3d correspond to Te 3d5/2 and Te 3d3/2, respectively (figure 2(e)) [33]. The spin-orbit separation of Te 3d5/2 and 3d3/2 is 10.2 eV. While the remaining two weak peaks at 573.3 eV and 583.7 eV indicate the presence of zero-valent Te [16]. According to the previously reported copper selenide, the Se 3d spectra of the as-synthesized Cu_2Se (figure 2(f)) exhibit two distinct peaks at 54.4 and 55.4 eV for Se $3d_{5/2}$ and $3d_{3/2}$, respectively [34]. In figure 2(g), the binding energies of S^{2-} in Cu_2S were measured to be 161.2 and 162.5 eV, with a 1.2 eV gap between them and an additional peak was detected at 168.6 eV which could be attributed to the partial oxidation of surface sulfur to SO_4^{2-} species [35]. The XPS peaks hence confirmed the formation of the copper chalcogenides containing Cu^{+2} and the chalcogenide anion.

The electrocatalytic activity for copper chalcogenides for OER was measured in a 1.0 M KOH alkaline solution using the Cu_2X-modified electrodes. Cu_2Te demonstrated the highest OER activity compared to the other Cu-chalcogenides, as shown in figure 3(a). Cu_2Te requires a low overpotential (η) of 255 mV to achieve the current density of 10 mA cm^{-2}. The other chalcogenides required an overpotential of 297, 334, 379 mV at 10 mA cm^{-2} for Cu_2Se, Cu_2S and Cu_2O, respectively as shown in figure 3(b).

The blank substrate did not show any OER activity as expected, confirming that the activity observed for the catalyst-loaded electrodes was solely due to the intrinsic catalytic activity of these Cu-chalcogenides. The OER electrocatalytic activity of the Cu-chalcogenides was also compared with that of state-of-the-art RuO_2 catalyst. The comparison of the LSV plots clearly demonstrated that all the copper chalcogenides have higher OER catalytic activity than RuO_2, while Cu_2O showed comparable activity. The kinetics of the OER activity was estimated from the Tafel plots by calculating the Tafel slope from the LSV plots near onset of the OER activity. The Tafel plot can also be used to determine the transfer coefficient, which is a measure of the rate of electron transfer between the electrode and the electrolyte.

The transfer coefficient is determined by the intercept of the Tafel plot on the x-axis. In figure 3(c), Cu_2O, Cu_2S, Cu_2Se and Cu_2Te exhibited the Tafel slope values of 138.61, 131.13, 126.43 and 74.28 mV dec^{-1}, respectively. Typically, lower Tafel slopes indicates faster electron transfer and more efficient catalytic activity. Comparison of Tafel slope for all the Cu-chalcogenides revealed that Cu_2Te shows the lowest value indicating most effective electrocatalytic activity. The stability of these catalysts was tested by carrying our continuous OER for several hours at constant applied potential through chronoamperometry studies. As shown in

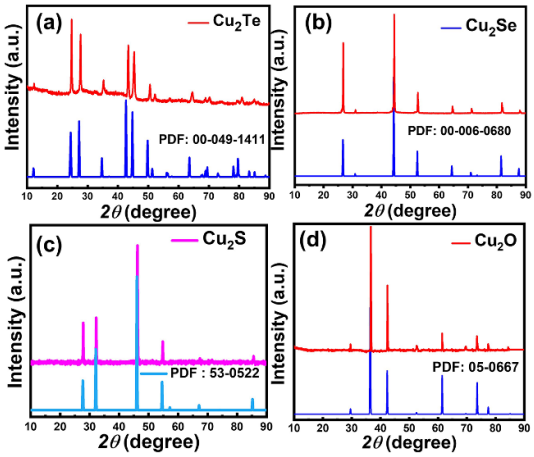

Figure 1. PXRD patterns for (a) Cu_2Te (b) Cu_2Se (c) Cu_2S, and (d) Cu_2O showing good agreement with the standard PXRD patterns as included in the respective plots.

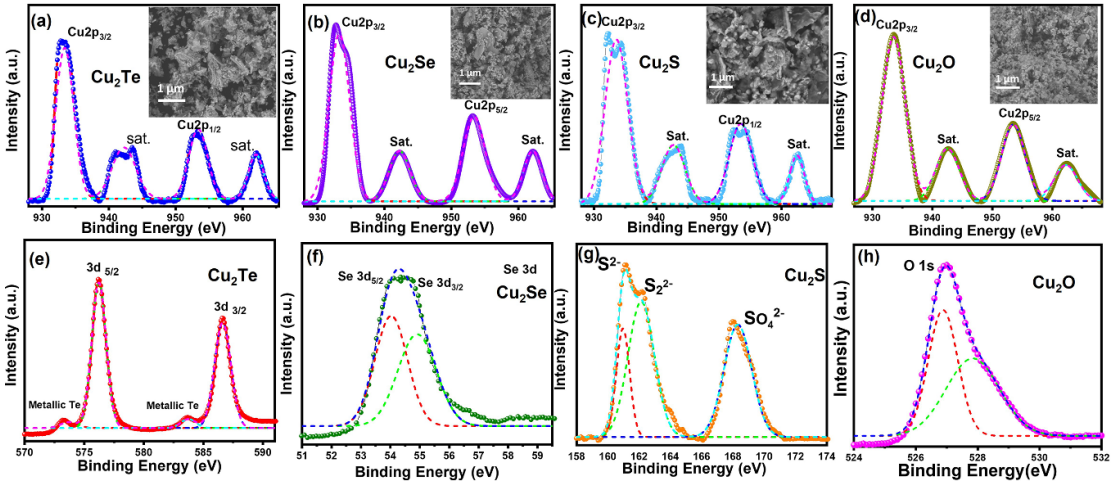

Figure 2. High resolution Cu2p XPS spectra for (a) Cu_2Te, (b) Cu_2Se, (c) Cu_2S and (d) Cu_2O, respectively. The chalcogen XPS peaks are shown in (e) Te 3d (Cu_2Te), (f) Se 3d (Cu_2Se) (g) S 2p (Cu_2S), and (h) O1s (Cu_2O). Insets in (a)–(d) shows the SEM images of Cu_2Te, Cu_2Se, Cu_2S and Cu_2O samples.

figure 4(a), the Cu_2Te catalyst demonstrated excellent stability over an extended period of time at different applied potentials of 1.49 V and 1.58 V vs RHE with minimum performance degradation. Also, the chronoamperometric measurements of the Cu_2Te material was measured at higher current densities of 260 mA cm^{-2} as shown in figure S1(a), to simulate real-world conditions more closely for water electrolysis. Following the extended testing protocol, it was observed that the Cu_2Te electrocatalyst indeed exhibits commendable stability for OER. After 24 h of continuous OER activity, only a minor deterioration of 4.233% was observed. A multi-step chronoamperometry test was also carried out to investigate stability of the catalysts at various current densities. Figure 4(b) shows the multistep chronoamperometry experiments conducted at range of constant applied potentials. Current density was measured for over two hours at each potential and the applied potentials were initially changed in ascending order from 1.36 V to 1.62 V against RHE, and subsequently in descending order from 1.62 V to 1.48 V vs RHE. As can be seen from figure 4(b), Cu_2Te showed stable current density at all applied potential in the forward and reverse potential sweep, confirming extensive cycling as well as operational stability. The overpotential change of Cu_2Te is negligible in the LSV curve obtained after 24 h of multistep chronoamperometry (figure 4(c)), further confirming the exceptional robustness of this catalyst. XPS and of the Cu_2Te were measured after 24 h of multistep chronoamperometry, in order to examine its compositional stability. XPS measured after long-term chronoamperometry (figure 4(d)) was found to be essentially unchanged when compared to that of the pristine sample, which indicates that the Cu_2Te catalyst composition was indeed stable for prolonged period of time. The post-OER XPS analysis of Cu_2Se and Cu_2S was also carried out and as shown in figure S2, they

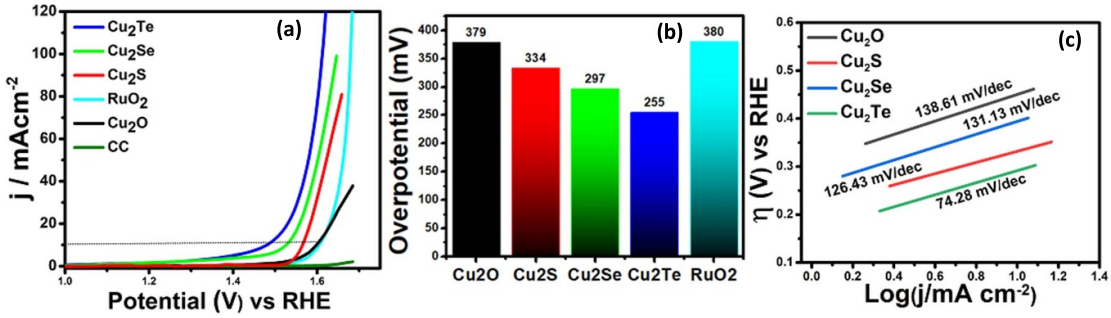

Figure 3. (a) LSV plots of Cu_2O, Cu_2S, Cu_2Se, Cu_2Te, RuO_2 and carbon cloth in 1 M KOH at a scan rate of 5 mV s^{-1}. (b) Comparison of OER overpotentials, and (c) Tafel plot of Cu_2O, Cu_2S, Cu_2Se and Cu_2Te catalysts.

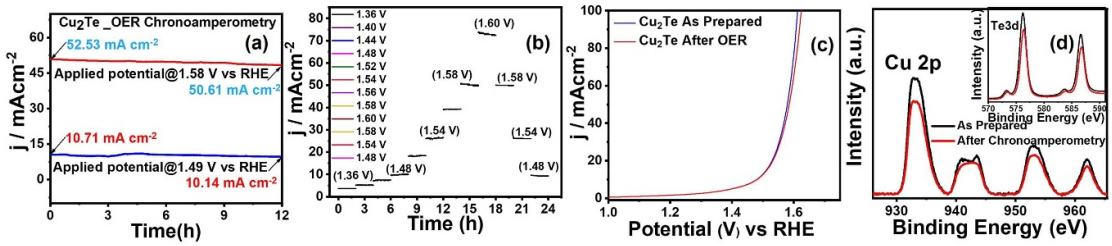

Figure 4. (a) Chronoamperometry at different applied potentials for Cu_2Te. (b) Multistep chronoamperometry at different applied potential steps (ascending and descending). (c) LSV of Cu_2Te before and after 24 h of multistep-chronoamperometry. (d) High resolution XPS spectra of Cu 2p, and Te 3d (inset) before and after multistep chronoamperometry.

do not show any major change in the Cu or S/Se peaks including changes in peak position, corresponding to retention of compositional integrity.

The electrochemical surface area (ECSA) is an essential parameter when evaluating the performance of electrocatalysts. It refers to the total active area available for electrocatalysis on the surface of an electrode. A higher ECSA usually implies more active sites available for the reaction, leading to enhanced catalytic activity. The ECSA of an electrode material can be significantly influenced by its composition, crystallinity, morphology, and particle size. In the case of the metal chalcogenides reported here (Cu_2Te, Cu_2Se, Cu_2S, and Cu_2O), the differences in ECSA can be attributed to their structural differences and material properties.

The ECSA was examined using cyclic voltammetry plots, scanned in the range from 0 to 0.25 V with scan rates between 25 – 200 $mV.s^{-1}$ in N_2 saturated 1 M KOH solution (figures 5(a)–(d). The anodic and cathodic currents were measured at 0.15 V vs Ag/AgCl for Cu_2Te, Cu_2Se, Cu_2S and 0.075 for Cu_2O as shown in figures 5(e)–(h) which shows the anodic and cathodic current plotted as a function of scan rates. The detailed calculation of ECSA has been described in the supplementary information file. Table S1 shows the ECSA value of each catalyst where Cu_2Te, has the highest ECSA (24.48), while Cu_2O, exhibit the lowest ECSA (9.36). Since the ECSA of these chalcogenides varies in the series, the ECSA-normalized current density has also been analyzed to compare the intrinsic catalytic activity across the series. As shown in figure S1(b), Cu_2Te electrode exhibited the highest current density and OER activity even after normalizing the LSV curves by ECSA. This observation unequivocally points to an enhancement in the intrinsic OER activity of the active sites due to variations in anion electronegativity, with Cu_2Te demonstrating the most superior activity.

Electroimpedance spectroscopy (EIS) was carried out to investigate the charge transfer rates at the various interfaces of the catalyst-electrode composite, specifically, the charge transfer resistance (R_{CT}) at the electrode–electrolyte interface. R_{CT} is critically dependent on the material composition and band-edge alignment of the electrocatalyst with the water-oxidation level. Hence, it is expected that R_{CT} will show variation as the catalyst composition changes between different chalcogenides. A lower R_{CT} depicts faster electron transfer at the electrode–electrolyte interface. The EIS spectra for all Cu-chalcogenides along with the equivalent circuit is shown in figure 6 while table 1 lists the estimated values for each component of the equivalent circuit derived from the Nyquist plots.

Comparison of the R_{CT} values showed that the Cu_2Te electrode exhibited a much lower charge transfer resistance (13.24) than that of Cu_2Se (24.6), Cu_2S (34.4), and Cu_2O (43.8) during the OER process. The trend of R_{CT} corroborates well with the observed OER activity which shows a gradual improvement on going from oxide to telluride. The transition metal tellurides are mostly metallic while their bandgap increases

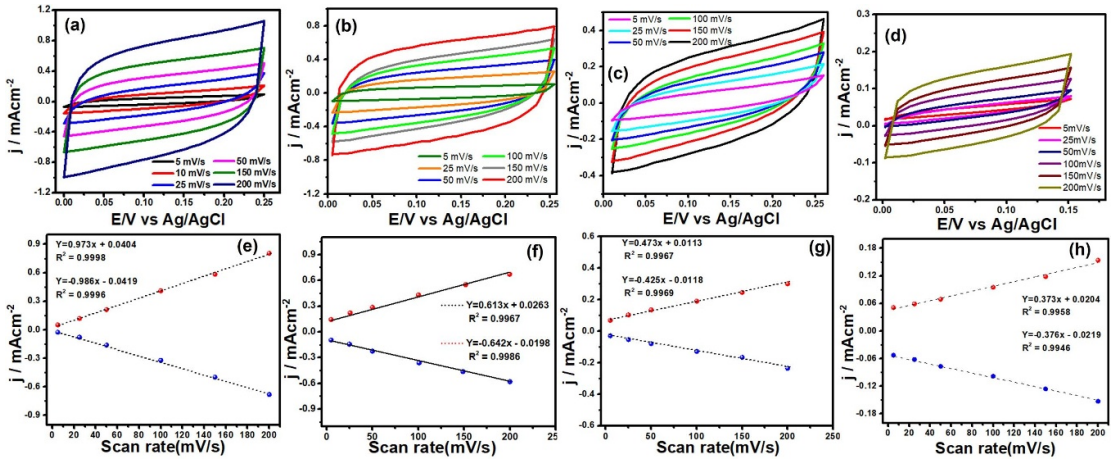

Figure 5. Cyclic voltammograms measured at different scan rates for (a) Cu_2Te, (b) Cu_2Se, (c) Cu_2S, and (d) Cu_2O. Plots of anodic and cathodic currents measured as a function of different scan rates for (e) Cu_2Te, (f) Cu_2Se, (g) Cu_2S, and (h) Cu_2O.

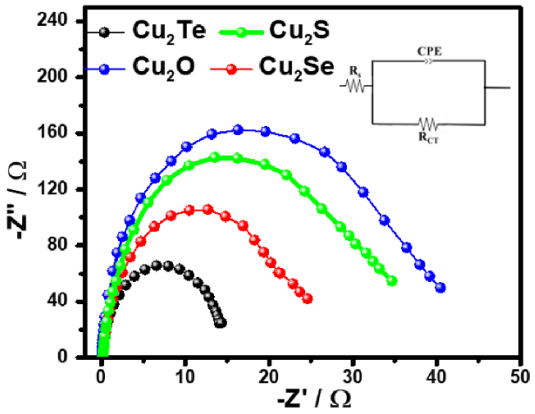

Figure 6. Nyquist impedance plots of as-synthesized Cu based catalysts. Inset represents the equivalent circuit model used for AC impedance fitting.

Table 1. Equivalent circuit parameters obtained from fitting of EIS experimental data.

Parameter	Value (Cu_2Te)	Value (Cu_2Se)	Value (Cu_2S)	Value (Cu_2O)
R_f/Ω	3.24	3.36	4.12	4.47
R_{ct}/Ω	13.24	24.63	34.41	43.80
$CPE_{catalyst}/F$	1.38	1.45	1.51	1.47
Z_W	1.71	1.84	1.96	2.32

from telluride to oxide. Hence, copper oxides typically have a larger bandgap compared to copper selenide, while copper telluride shows metallic character. The metallic character in the tellurides enhances electron transfer within the catalyst composite as well as at the electrode–electrolyte interface, thereby, improving the electrocatalytic activity. A comparison with other Cu-based chalcogenides showed that the as-synthesized Cu_2Te demonstrated highest catalytic activity (table 2).

Calculations based on DFT were carried out in order to acquire additional insights of the OER mechanism on the copper chalcogenide surfaces and understand the enhanced activity of the copper telluride. Conventionally OER in basic medium involves four elementary steps on the catalytically active transition metal sites on the surface, generating three different intermediate adsorbates: *OH, *O, and *OOH (the asterisk denotes the adsorption site). Figure 7 shows the calculated free energy profiles of the different OER steps on the Cu site in Cu_2Te. Apparently, the highest energy barrier is observed for the formation of dioxygen species from hydroperoxide. However, these energy profiles represent adsorption of a single oxygenated species on the catalytically active site and provides a good estimation of the adsorption energies that can be compared between different catalytic surfaces. It should also be noted that in the actual OER mechanism on the catalyst surface, the oxygenated intermediates are expected to adsorb on all exposed

Table 2. Comparison of OER performance for various of copper-based catalysts.

OER catalysts	Electrolytes	η @ 10 mA cm^{-2} (mV *vs* RHE)	Tafel slope mV dec $^{-1}$	References
Cu_2Se	1 M KOH	270	48.1	[36]
CuO from Cu–EA	1 M KOH	475	90	[37]
CuO-A/CF	1 M KOH	297	72.8	[38]
CuO_Nps	1 M NaOH	290	89	[39]
Cu(dto)/C	1 M KOH	400	81	[40]
CuSe/NF	1 M KOH	297	89	[41]
Cu_7Te_4 nanosheets	1 M KOH	323	145	[42]
Cu_7Te_4-NW	1 M KOH	277	33	[43]
Cu_2S-CF	1 M KOH	309	70	[44]
Cu_2S/Cu	1 M KOH	373	50	[45]
Cu_7Te_4-Nanosheet	1 M KOH	442	176	[42]
Cu_2O	**1 M KOH**	**379**	**138.61**	**This Work**
Cu_2S	**1 M KOH**	**334**	**131.13**	**This Work**
Cu_2Se	**1 M KOH**	**297**	**126.43**	**This Work**
Cu_2Te	**1 M KOH**	**255**	**74.28**	**This Work**

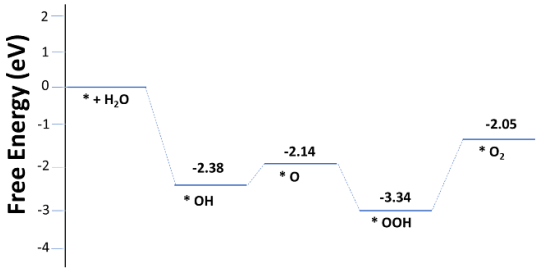

Figure 7. The calculated OER free energy diagram on Cu_2Te surface.

catalytic sites on the surface, leading to build up of excess negative charge and electron density on the surface. Accumulation of such high electron density and the resulting electric field near the surface will effectively lead to variation of the adsorption energies from this ideal scenario. Hence the actual rate determining step on a fully covered catalyst surface should rather be determined experimentally through Tafel slope analysis. In the present study, Cu_2Te shows a Tafel slope value corresponding to the 2nd electron transfer step (formation of *O) being the rate determining step. Formation of *O and all other oxygenated intermediates on the catalyst surface critically depends on the surface coverage of the catalyst site with hydroxyl (–OH) group which is considered as the catalyst activation step. Hence, DFT calculation were also performed on the all Cu-chalcogenide surfaces to investigate the catalyst surface activation through adsorption of hydroxyl (–OH) group on the catalytic site. Previous report including both theoretical and experimental studies have shown that the adsorption of oxygenated intermediates (particularly *OH) is the most energy-intensive part of the water oxidation process [3].

In our previous studies we have proposed that the –OH adsorption energy can be used as an appropriate descriptor for OER catalytic efficiency [18, 46, 47], especially since the OER mechanism involves intermediate adsorption and desorption from only the catalytic site without forming a bridging connection with neighboring lattice sites. We have used DFT calculations to estimate the OH adsorption energy on the Cu sites of (001) lattice planes in Cu_2O, Cu_2S, Cu_2Se, and Cu_2Te as shown in figure 8. In order to perform the calculation of the OH–adsorption energy, first the surfaces were relaxed to obtain the energy of the clean surfaces. Then OH–ions were placed on top of the active metal site, and the system was relaxed to calculate the total formation energy of the system. The relaxed surface of Cu_2Te and other copper-based systems after the OH—attachment on the (001) surface is shown in figure S3. The adsorption energy of OH–ions, E_{ad}, was derived as $E_{ad} = E_{sys} – E_{clean} – E_{OH}$, where E_{OH} is the energy of free OH^-. The OH adsorption energy on the (001) surface of Cu_2O, Cu_2S, Cu_2Se, and Cu_2Te was found to be −1.095, −1.76, −2.075 2.38 eV, respectively, as indicated in figure 8(a). The higher OH adsorption energy on Cu_2Te surface suggests that catalyst activation and surface coverage by OH is more favorable on Cu_2Te surface. Typically, the activation of the catalyst comprises attachment of the hydroxide ion to the surface, which initiates OER [48, 49]. We have further correlated the –OH adsorption energy with the observed overpotential by constructing a volcano-type plot as shown in figure 8(b). Along with Cu-chalcogenides, several other high-efficiency OER

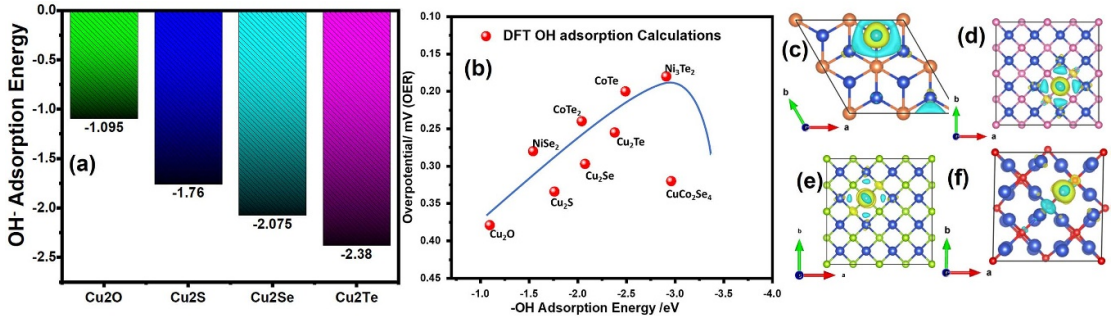

Figure 8. (a) Comparison of the calculated –OH adsorption energy of Cu site in Cu_2O, Cu_2S, Cu_2Se, and Cu_2Te (001) surfaces. (b) Overpotential *vs* OH adsorption energy plots for various OER catalysts, revealing a volcano-type relationship. Schematic representation of the charge density difference before and after –OH adsorption on (c) Cu_2Te (d) Cu_2Se, (e) Cu_2S, (f) Cu_2O, surfaces (yellow: reduced electron density; cyan: excess electron density).

electrocatalyst has been compared in the volcano plot as shown in figure 8(b). Interestingly it was observed that the –OH adsorption energy indeed shows a gradual increase as a function of decreasing anion electronegativity corresponding to enhancement of OER activity (reducing overpotential). These observations across many Cu, Co, and Ni-based catalysts confirm that the OH adsorption energy on the catalyst surface can indeed serve as a simple descriptor for OER activity.

Figure S4 shows the partial density of states for the Cu 3d-state before and after OH attachment. Here the occupied spin-up and spin-down Cu states move to the lower negative energy state upon bonding with OH^-, as a result of the weaker Cu–Te interactions. In addition, the attachment of the OH ion to Cu_2Te surfaces results in a redistribution of charges because of electronic hybridization between the orbitals of the adsorbate and the adsorbent. Charge density redistribution frequently occurs in conjunction with adsorption. As a result, we have used charge analysis to investigate the charge density difference in order to interpret the adsorption mechanism. Figures 8(c)–(f) depict the differential charge densities of adsorbed OH on Cu sites of and Cu_2Te, Cu_2Se, Cu_2S, Cu_2O and respectively. According to the integrated charge density difference, the Cu–OH layer is surrounded by an apparent electron accumulation at Cu atoms (sky-blue region) and an electron reduction at O atoms (yellow region), leading to new electronic states at the Cu–OH heterointerface. The largest electron cloud, depicted in figure 8(c), indicates a high rate of electron transfer and robust contact between $^*OH$ and the Cu_2Te catalyst surface; this is supported by the value of the adsorption energy, which is negative (−2.38 eV).

5. Conclusion

To summarize, the effect of anion electronegativity in improving OER catalytic activity was confirmed through a systematic investigation of the copper chalcogenide series. Cu_2Te showed the lowest overpotential compared to Cu_2Se, Cu_2S, and Cu_2O depicting best OER efficiency. DFT calculations revealed that the enhanced activity could be attributed to the facile –OH adsorption on the catalytic site in Cu_2Te. It also confirmed that the –OH adsorption energy on single catalyst site can be used an appropriate descriptor for the observed OER catalytic efficiency. Such insight regarding the effect of anion electronegativity and possibility of using the adsorption energy as a descriptor for predicting catalytic efficiency will be extremely useful for optimal catalyst surface design.

Data availability statement

All data that support the findings of this study are included within the article (and any supplementary files).

Acknowledgments

Financial support was provided through NSF grants, CAS2102609 and CAS2155175. DFT calculations were performed at the Molecular Foundry supported through standard user proposal (#7804). Authors would like to acknowledge MRC for equipment usage.

ORCID iD

Manashi Nath https://orcid.org/0000-0002-5058-5313

References

[1] Suen N T, Hung S F, Quan Q, Zhang N, Xu Y J and Chen H M 2017 Electrocatalysis for the oxygen evolution reaction: recent development and future perspectives *Chem. Soc. Rev.* **46** 337–65

[2] Jo S, Lee K B and Sohn J I 2021 Direct electrosynthesis of selective transition-metal chalcogenides as functional catalysts with a tunable activity for efficient water electrolysis *ACS Sustain. Chem. Eng.* **9** 14911–7

[3] Nath M, Singh H and Saxena A 2022 Progress of transition metal chalcogenides as efficient electrocatalysts for energy conversion *Curr. Opin. Electrochem.* **34** 100993

[4] Nguyen T X, Su Y-H, Lin C-C, Ting J-M, Nguyen T X, Su Y-H, Lin C-C and Ting J-M 2021 Self-reconstruction of sulfate-containing high entropy sulfide for exceptionally high-performance oxygen evolution reaction electrocatalyst *Adv. Funct. Mater.* **31** 2106229

[5] Zhu Y, Chen H C, Hsu C S, Lin T S, Chang C J, Chang S C, Tsai L D and Chen H M 2019 Operando unraveling of the structural and chemical stability of P-substituted CoSe 2 electrocatalysts toward hydrogen and oxygen evolution reactions in alkaline electrolyte *ACS Energy Lett.* **4** 987–94

[6] Li W, Xiong D, Gao X, Liu L, Li R and Article F 2019 The oxygen evolution reaction enabled by transition metal phosphide and chalcogenide pre-catalysts with dynamic changes *Chem. Commun.* **55** 8744–63

[7] Xie X *et al* 2022 Oxygen evolution reaction in alkaline environment: material challenges and solutions *Adv. Funct. Mater.* **32** 2110036

[8] Singh H, Liyanage W P R, Nath M, Li R and Communication C 2022 Carbon nanotube encapsulated metal selenide nanostructures for efficient electrocatalytic oxygen evolution reaction *Chem. Commun.* **58** 8360–3

[9] Voiry D, Yang J, Chhowalla M, Voiry D, Yang J and Chhowalla M 2016 Recent strategies for improving the catalytic activity of 2D TMD nanosheets toward the hydrogen evolution reaction *Adv. Mater.* **28** 6197–206

[10] Singh H, Bernabe J, Chern J and Nath M 2021 Copper selenide as multifunctional non-enzymatic glucose and dopamine sensor *J. Mater. Res.* **36** 1413–24

[11] Saxena A, Liyanage W, Kapila S and Nath M 2022 Nickel selenide as efficient electrocatalyst for selective reduction of carbon dioxide to carbon-rich products *Catal. Sci. Technol.* **12** 4727–39

[12] Huang Y, Jiang L W, Shi B Y, Ryan K M and Wang J J 2021 Highly efficient oxygen evolution reaction enabled by phosphorus doping of the fe electronic structure in iron–nickel selenide nanosheets *Adv. Sci.* **8** 2101775

[13] Yi P, Song Y, Li C, Liu R and Sun J 2023 Heterostructured Mn-doped NiSx/NiO/Ni3N nanoplate arrays as bifunctional electrocatalysts for energy-saving hydrogen production and urea degradation *Appl. Surf. Sci.* **619** 156789

[14] Wu Y Z, Huang Y, Jiang L W, Meng C, Yin Z H, Liu H and Wang J J 2023 Modulating the electronic structure of CoS_2 by Sn doping boosting urea oxidation for efficient alkaline hydrogen production *J. Colloid Interface Sci.* **642** 574–83

[15] Coughlan C, Ibáñez M, Dobrozhan O, Singh A, Cabot A and Ryan K M 2017 Compound copper chalcogenide nanocrystals *Chem. Rev.* **117** 5865–6109

[16] Nath M, Silva De U, Singh H, Perkins M, Liyanage W P R, Umapathi S, Chakravarty S and Masud J 2021 Cobalt telluride: a highly efficient trifunctional electrocatalyst for water splitting and oxygen reduction *ACS Appl. Energy Mater.* **4** 1c01438

[17] Umapathi S, Masud J, Swesi A T and Nath M 2017 $FeNi_2Se_4$ –reduced graphene oxide nanocomposite: enhancing bifunctional electrocatalytic activity for oxygen evolution and reduction through synergistic effects *Adv. Sustain. Syst.* **1** 1700086

[18] De Silva U, Masud J, Zhang N, Hong Y, Liyanage W P R, Asle Zaeem M and Nath M 2018 Nickel telluride as a bifunctional electrocatalyst for efficient water splitting in alkaline medium *J. Mater. Chem.* A **6** 7608–22

[19] De Silva U, See J, Liyanage W P R, Masud J, Wu J, Yang W, Chen W-T, Prendergast D and Nath M 2021 Understanding the structural evolution of a nickel chalcogenide electrocatalyst surface for water oxidation *Energy Fuels* **35** 4403

[20] Cao X, Johnson E and Nath M 2019 Identifying high-efficiency oxygen evolution electrocatalysts from Co–Ni–Cu based selenides through combinatorial electrodeposition *J. Mater. Chem.* A **7** 9877–89

[21] Saxena A, Singh H and Nath M 2022 Cobalt telluride electrocatalyst for selective electroreduction of CO_2 to value-added chemicals *Mater. Renew. Sustain. Energy* **2022** 1–15

[22] Lu S, Shi Y, Zhou W, Zhang Z, Wu F and Zhang B 2022 Dissolution of the heteroatom dopants and formation of ortho-quinone moieties in the doped carbon materials during water electrooxidation *J. Am. Chem. Soc.* **144** 3250–8

[23] Rana S, Yadav K K, Sunaina, Mehta S K and Jha M 2022 Structurally engineered anisotropic cobalt-based nanostructures for efficient chlorine and oxygen evolution *Adv. Mater. Interfaces* **9** 2200740

[24] Li G, Tang Y, Fu T, Xiang Y, Xiong Z, Si Y, Guo C and Jiang Z 2022 S, N co-doped carbon nanotubes coupled with CoFe nanoparticles as an efficient bifunctional ORR/OER electrocatalyst for rechargeable Zn-air batteries *Chem. Eng. J.* **429** 132174

[25] Singh H, Marley-Hines M, Chakravarty S and Nath M 2022 Multi-walled carbon nanotube supported manganese selenide as highly active bifunctional OER and ORR electrocatalyst *J. Mater. Chem.* A **6** 4883–5230

[26] Mishra P, Singh D, Sonvane Y and Ahuja R 2022 Bifunctional catalytic activity of 2D boron monochalcogenides BX (X = S, Se, Te) *Mater. Today Energy* **27** 101026

[27] Sadaqat M, Manzoor S, Aman S, Gouadria S, Usman M, Joya K S, Najam-Ul-Haq M, Hassan H M A, Ashiq M N and Taha T A 2022 Mn-based hierarchical polyhedral 2D/3D Nanostructures MnX2(X = S, Se, Te) derived from mn-based metal-organic frameworks as high-performance electrocatalysts for the oxygen evolution reaction *Energy Fuels* **36** 10327–38

[28] Mabayoje O, Shoola A, Wygant B R and Mullins C B 2016 The role of anions in metal chalcogenide oxygen evolution catalysis: electrodeposited thin films of nickel sulfide as "pre-catalysts" *ACS Energy Lett.* **1** 195–201

[29] Ooka H, Huang J and Exner K S 2021 The sabatier principle in electrocatalysis: basics, limitations, and extensions *Front. Energy Res.* **9** 155

[30] Kresse G and Furthmüller J 1996 Efficient iterative schemes for *ab initio* total-energy calculations using a plane-wave basis set *Phys. Rev.* B **54** 11169

[31] Perdew J P, Burke K and Ernzerhof M 1996 Generalized gradient approximation made simple *Phys. Rev. Lett.* **77** 3865

[32] Perdew J P, Chevary J A, Vosko S H, Jackson K A, Pederson M R, Singh D J and Fiolhais C 1992 Atoms, molecules, solids, and surfaces: applications of the generalized gradient approximation for exchange and correlation *Phys. Rev.* B **46** 6671

[33] Li Q, Rao H, Ma X, Mei H, Zhao Z, Gong W, Camposeo A, Pisignano D and Yang X 2022 Unusual red light emission from nonmetallic Cu2Te microdisk for laser and SERS applications *Adv. Opt. Mater.* **10** 2101976

[34] Umapathi S, Singh H, Masud J and Nath M 2020 Nanostructured copper selenide as an ultrasensitive and selective non—enzymatic glucose sensor *Mater. Adv.* **2** 927–32

[35] Kim C S, Choi S H and Bang J H 2014 New insight into copper sulfide electrocatalysts for quantum dot-sensitized solar cells: composition-dependent electrocatalytic activity and stability *ACS Appl. Mater. Interfaces* **6** 22078–87

[36] Masud J, Liyanage W P R, Cao X, Saxena A and Nath M 2018 Copper selenides as high-efficiency electrocatalysts for oxygen evolution reaction *ACS Appl. Energy Mater.* **1** 4075–83
[37] Liu X, Cui S, Qian M, Sun Z and Du P 2016 In situ generated highly active copper oxide catalysts for the oxygen evolution reaction at low overpotential in alkaline solutions *Chem. Commun.* **52** 5546–9
[38] Wang X, Hou X, Lee H, Lu L, Wu X and Sun L 2020 Copper selenide–derived copper oxide nanoplates as a durable and efficient electrocatalyst for oxygen evolution reaction *Energy Technol.* **8** 2000142
[39] Huan T N, Rousse G, Zanna S, Lucas I T, Xu X, Menguy N, Mougel V and Fontecave M 2017 A dendritic nanostructured copper oxide electrocatalyst for the oxygen evolution reaction *Angew. Chem., Int. Ed.* **56** 4792–6
[40] Putra R P, Horino H and Rzeznicka I I 2020 An efficient electrocatalyst for oxygen evolution reaction in alkaline solutions derived from a copper chelate polymer via in situ electrochemical transformation *Catalysts* **10** 233
[41] Chakraborty B, Beltrán-Suito R, Hlukhyy V, Schmidt J, Menezes P W and Driess M 2020 Crystalline copper selenide as a reliable non-noble electro(pre)catalyst for overall water splitting *ChemSusChem* **13** 3222–9
[42] Wang R, Liu Y, Tian Z, Shi Y, Xu Q, Zhang G, Chen J and Zheng W 2020 Copper telluride Nanosheet/Cu foil electrode: facile ionic liquid-assisted synthesis and efficient oxygen evolution performance *J. Phys. Chem.* C **124** 22117–26
[43] Hassan A, Nisar L, Iqbal R, Sadaqat M, Hussain F, Ashiq M N, Najam-ul-Haq M, Shah A and Joya K S 2021 Copper telluride nanowires for high performance electrocatalytic water oxidation in alkaline media *J. Power Sources* **491** 229628
[44] Du J, Qian Y, Wang L, Yang H and Kang D J 2020 Facile synthesis of copper sulfides on copper foam as an efficient electrocatalyst for oxygen evolution reaction *Mater. Today Commun.* **25** 101585
[45] Sun J, Zhou H, Song P, Liu Y, Wang X, Wei T, Shen X, Chen P and Zhu G 2021 Cuprous sulfide derived CuO nanowires as effective electrocatalyst for oxygen evolution *Appl. Surf. Sci.* **547** 149235
[46] Cao X, Medvedeva J E and Nath M 2020 Copper cobalt selenide as a high-efficiency bifunctional electrocatalyst for overall water splitting: combined experimental and theoretical study *ACS Appl. Energy Mater.* **3** 3092–103
[47] De Silva U, See J, Liyanage W P R, Masud J, Wu J, Yang W, Chen W T, Prendergast D and Nath M 2021 Understanding the structural evolution of a nickel chalcogenide electrocatalyst surface for water oxidation *Energy Fuels* **35** 4387–403
[48] X P L, Huang C, Han W K, Ouyang T and Liu Z Q 2021 Transition metal-based electrocatalysts for overall water splitting *Chin. Chem. Lett.* **32** 2597–616
[49] Sun J, Zhao Z, Li J, Li Z and Meng X 2022 Recent advances in transition metal selenides-based electrocatalysts: rational design and applications in water splitting *J. Alloys Compd.* **918** 165719